Proposal of a simplified analytical approach for the characterisation of the end-plate component in circular tube connection

Hoang Van-Long, Demonceau Jean-François, Jaspart Jean-Pierre

ArGEnCo Department, Liège University, Belgium

Abstract: This paper presents a study realised at Liège University on the behaviour of the rectangular end-plate in bending and the bolt in tension components met in circular tube-to-circular tube connections and in circular tubular column bases. Analytical formulas for the mentioned components are firstly proposed considering different yield line patterns for the end-plate. Then the results predicted through the proposed analytical approach are validated through comparisons to experimental and finite element results. Finally, the application of the proposed approach for the prediction of the strength of tube-to-tube joints and also for the prediction of the bolt force of column bases is demonstrated.

Key words: Bolted end-plate connections; Column bases; Circular tube structures; Yield line analysis; Experimental tests; Finite element analysis.

Highlights

- The component “end-plate in bending” met in tubular construction is investigated
- Analytical formulas for the prediction of the strength of this component is proposed
- These formulas are validated through comparisons to experimental and FEM results
- How these formulas can be used to predict the connection strength is described
- It is shown how they can be used to predict the bolt tensile loads in column bases

1. Introduction

Bolted connections using end-plates is one of efficient solutions for steel structures using tubular members, as buildings, bridges, offshores, etc. This type of connection can be used in member-to-member joints or in column bases. However, regarding the literature, most of developments have been devoted to welded connections (e.g [1, 2]) and the design rules are available in codes (e.g [3]), the same observation cannot be drawn for bolted end-plate connections. The developments on the bolted end-plate connection with circular tube members are therefore necessary, on which the key is the behaviour of the “end-plate in bending” component.

In the Eurocodes [3], the behaviour of the component "end-plate in bending" is characterised through the definition of equivalent T-stub, identifying for the latterthree failure modes (I, II and III). For the definition of the equivalent T-stub, the effective lengths representing the "length" of the equivalent T-stub needed to be defined; these effective lengths are directly linked to the development of plastic yield lines within the end-plate when the column subjected to bending or tension.

Researches on the component "end-plate in bending" for joints with I/H shaped members has been widely developed in the last decades (e.g. [4, 5, 6, 7]) and is covered in Eurocode-3, part 1-8 [3]. Also, the behaviour of end-plate in connections between rectangular hollow members has been studied by Wald et al [8]; in particular, effective lengths for the definition of equivalent T-stub for such connections are proposed and analytical formulas to predict these effective lengths are given. These formulas have been recently generalized to the case of column basis joints of circular tubular columns by Horová et al [9]. However, the considered yielding patterns for the definition of the effective lengths are limited as only one straight line is supposed for the failure mechanism (per bolt), and the possible bolt group effect is omitted in Wald and Horová works [8,9]. In another research, a model for designing end-plate connections using rectangular hollow sections with four bolts has been proposed by Wheeler et al [10], in which more sophisticated yielding patterns, with multi straight yield lines, are considered. Wheeler et al [11] also generalized their models to the case of connections between rectangular hollow members with eight bolts. However, Wheeler models [10,11] are not yet extended to the case of circular tubular members.

In this paper, a model for the characterisation of end-plates welded to circular tubular members is proposed. Both tube-to-tube joints and column bases using rectangular end plate with four bolts are considered (Fig.1). Yielding patterns with multi straight yield lines, taking into account the possible bolt group effect, are considered for the end-plate in bending (Sections 2.1 and 2.2). Analytical formulas for new yield line patterns are derived and then validated through comparisons to experimental and finite element (FE) results (Sections 2.3 and 2.4). The application of the proposed formulas to predict the strength of the tube-to-tube joints and the bolt forces in column bases is also presented in Section 3.

2. Characterisation of the components "end-plate in bending" and "bolts in tension"

2.1. Generalities

This section aims at computing the plastic strength of the system shown in Fig.2a by using the kinematical approach of limit analysis. In the model, a rigid-plastic approach is used

for the end plate and the bolts while the foundation and the tube are assumed to be infinitely rigid.

A straight yield line throughout the plate is supposed in the compression zone while different configurations of yield lines are contemplated for the tension zone (Fig.3). The limit load corresponding to the yielding line patterns given in “a”, “b”, “c” and “f” in Fig.3 can be found in the literature, e.g. [5], while the one corresponding to “d” and “e” is not yet covered and is studied in the following sections. It will be illustrated later on that the yield patterns “b”, “c” “e” and “f” may be considered as particular cases of the yielding pattern “d”.

The parameters which will be used for the development are listed here after (the geometrical parameters are given in Fig.2):

f_y is the yield strength of the end-plate steel

f_{yb} is the yield strength of the bolt material

f_u is the nominal ultimate tensile strength of the end-plate steel

M is the applied bending moment to the connection

r_o is the outside radius of the tube

r is the outside diameter of the tube including the weld, so $r = r_0 + 2(0,8a\sqrt{2})$

m_p is the unit plastic moment of the end plate ($m_p = 0.25 t_p^2 f_y$)

m_u is the unit ultimate moment of the end plate ($m_u = 0.25 t_p^2 f_u$)

B_p is the resistant plastic load per bolt ($B_p = A_s f_{yb}$ with A_s, the net tensile area of the bolt shank)

B_u is the ultimate load per bolt (the value can be found in Eurocode-3, part 1-8 [3])

2.2. Solution for yield pattern “d”

Fig.4 gives the detailed geometry of mechanism “d”. In fact, yield pattern “d” may be considered as a family of mechanisms which are governed by the position of point B on the y axis (or the position of the point A on x axis). For mechanism “d”, six (6) yield lines are formed and the end-plate is devised into four (4) rigid planes (Fig.4): plane 0 (contact surface, Fig.4a), plane 1 (DBB’), plane 2 (ABD), and plane 3 (AB’D). The aim is to find an optimal mechanism that absorbs a minimal energy which will correspond to the actual mechanism; this can be achieved by identifying the optimal position of point B (or A).

The starting point is the virtual work principle as written in Eq.(1):

$$W_E = W_I \tag{1}$$

where W_E is the external work depending of the virtual rotation φ as given in Eq.(2) and W_I the internal work given in Eq.(3):

$$W_E = M\varphi, \tag{2}$$

$$W_I = m_p \sum \theta_{ij} l_{ij} . \tag{3}$$

In Eq. (3), θ_{ij} and l_{ij} are the rotations and the lengths of the yield line between the plane *i* and the plane *j*, respectively. They may be computed using Eqs.(4) and (5):

$$l_{ij} = \sqrt{l_{ij,x}^2 + l_{ij,y}^2} \tag{4}$$

$$\theta_{ij} \approx \frac{\mathbf{n}_i \times \mathbf{n}_j}{\mathbf{n}_i \bullet \mathbf{n}_j} \tag{5}$$

In Eq.(4), $l_{ij,x}$ and $l_{ij,y}$ are of the projections of l_{ij} on the x and y axes, respectively. $\mathbf{n}_i$ and $\mathbf{n}_j$ in Eq.(5) are the normal vectors of plane *i* and plane *j* respectively. The formulas to determine $l_{ij,x}$, $l_{ij,y}$, $\mathbf{n}_i$ and $\mathbf{n}_j$ are presented in Table 1.

All the coordinates (x,y) of points A, C, D, E and F (see Table 1) can be written as a function of y_B, as given in Table 2.

Accordingly, using Eqs. (1) to (5), the applied moment can be now written as

$$M = W_I(y_B), \tag{6}$$

and the optimal mechanism may be obtained by solving the following problem (Eq.(7)):

$$\frac{dW_I}{dy_B} = 0 \rightarrow \text{optimal mechanism} \tag{7}$$

In principle, the analytical solution of Eq.(7) can be determined but its explicit form is quite complicated and not suitable for a direct application in practice. However, the problem of Eq.(7) can be easily solved through computer program with automatic calculations. For practical purpose, an approximate solution is proposed and presented in Section 2.3. Also, a computer program solving Eq.(7) was implemented to obtain the optimal solutions; the latter are validated through comparisons to experimental and FE results (Section 2.4.1). Finally, these optimal solutions are used to assess the proposed approximate solution (Section 2.4.2).

2.3. Approximate solution for "d" mechanism

To obtain a simplified analytical formulas, the following assumption is made (Fig.5): the inclined yield line HD (Fig.4b) is tangent to the tube (i.e. tangent to the outside surface of the tube taking into account of the welds) and perpendicular to the line passing by the bolt centre and the tube centre. With this simplification, the yield line pattern is defined and the plastic moment (Eq.(6)) is explicitly obtained, meaning that Eq.(7) is automatically satisfied.

The different equations for the different possible failure mode are as follows.

Plastic moment for a failure mode I (thin plate, Fig.3d):

$$M_p^I = (\theta_{01} l_{01} + \theta_{12} l_{12} + \theta_{20} l_{20} + \theta_{23} l_{23}) m_p \,. \tag{8}$$

Plastic moment for a failure mode II (intermediate plate, Fig.3e):

$$M_p^{II} = (\theta_{01} l_{01} + \theta_{12} l_{12} + \theta_{23} l_{23}) m_p + 2\delta_b B_p \,. \tag{9}$$

Plastic moment for a failure mode III (thick plate, Fig.3f):

$$M_p^{III} = \theta_{01} l_{01} m_p + 2\delta_b^{III} B_p \,. \tag{10}$$

It would to note that in the failure modes II and III (Eqs. (9) and (10)) the yields of the bolts in tension are considered.

The rotations and the lengths of the yield lines in Eqs. (8), (9) and (10) are obtained as follows.

- Rotations of the yield lines (Eq.(11) to Eq.(14)):

$$\theta_{10} = 1; \tag{11}$$

$$\theta_{12} = \frac{h + r - e_h}{\sqrt{(h - e_h)^2 + (b - e_b)^2} - r}; \tag{12}$$

$$\theta_{02} = \frac{1 + \sin\beta}{\sin\alpha \cos\beta (\tan\alpha \tan\beta + \tan\beta / \cos\alpha - 1/\sin\alpha - 1)}; \tag{13}$$

$$\theta_{23} = \frac{2\tan\beta (1 + 1/\sin\alpha)}{\tan\alpha \tan\beta + \tan\beta / \cos\alpha - 1/\sin\alpha - 1}. \tag{14}$$

- Length of the yield lines (Eq.(15) to Eq.(18)):

$$l_{01} = 2b; \tag{15}$$

$$l_{12} = l_{12,1} + l_{12,2} \text{ with } \begin{vmatrix} l_{12,1} = (b - r\cos\alpha)/\sin\alpha \text{ if } r(\tan\alpha + 1/\cos\alpha) \geq b \\ l_{12,1} = r(\tan\alpha + 1/\cos\alpha) \text{ if } r(\tan\alpha + 1/\cos\alpha) < b \\ l_{12,2} = r/\tan\alpha \text{ if } r/\sin\alpha \leq h \\ l_{12,2} = (h - r\sin\alpha)/\cos\alpha \text{ if } r/\sin\alpha > h \end{vmatrix}; \tag{16}$$

$$l_{02} = l_{02,1} + l_{02,2} \text{ with } \begin{vmatrix} l_{02,1} = e_b / \cos\beta \text{ if } r(\tan\alpha + 1/\cos\alpha) \geq b \\ l_{02,1} = (h + r - e_h) / \sin\beta \text{ if } r(\tan\alpha + 1/\cos\alpha) < b \\ l_{02,2} = e_h / \sin\beta \text{ if } r(\tan\alpha + 1/\cos\alpha)\tan\beta \geq h + r \\ l_{02,2} = (b - e_b) / \cos\beta \text{ if } r(\tan\alpha + 1/\cos\alpha)\tan\beta < h + r \end{vmatrix} ; \quad (17)$$

$$l_{23} = \begin{vmatrix} 0 \text{ if } r/\sin\alpha \geq h \\ h - r\sin\alpha \text{ if } \begin{cases} r/\sin\alpha \leq h \\ r(\tan\alpha + 1/\cos\alpha)\tan\beta \geq h + r \end{cases} \\ r(\tan\alpha + 1/\cos\alpha)\tan\beta - r(1 + 1/\sin\alpha) \text{ if } \begin{cases} r/\sin\alpha < h \\ r(\tan\alpha + 1/\cos\alpha)\tan\beta < h + r \end{cases} \end{vmatrix} . \quad (18)$$

- The elongations of the bolts for failure modes II and III are respectively given by Eq.(19) and Eq.(20):

$$\delta_b^{II} = e_b \sin\gamma + e_h \cos\gamma ; \quad (19)$$

$$\delta_b^{III} = h + r - e_h ; \quad (20)$$

The angles α, β and γ (Fig.5) are calculated through (Eq.(21) to Eq.(23)):

$$\alpha = \arctan\left(\frac{h - e_h}{b - e_b}\right); \quad (21)$$

$$\beta = \arctan\left(\frac{h + r - e_h}{r(\tan\alpha + 1/\cos\alpha - (b - e_b))}\right); \quad (22)$$

$$\gamma = \arctan\left(\frac{h + r}{r(\tan\alpha + 1/\cos\alpha)}\right). \quad (23)$$

2.4. Validation

2.4.1. Validation of the optimal solution through experimental results and numerical analysis

Experimental tests: In the framework of ATTEL project ("Performance-based approaches for high-strength tubular columns and connections under earthquake and fire loadings"), three specimens for the connection type shown in Fig.1b were tested at the University of Thessaly; the detail results can be found in [12]. The main properties of the specimens are presented in Table 3; the parameter which was varied for the test campaign is the thickness of the end-plate. The test set-up is given in Fig.6; according to the external load acting on the specimens, it can be assumed that the connection is subjected to pure bending moment. Fig.7 shows Specimen 1 after testing; the same deformation was observed for Specimens 2 and 3. So failure mode I can be identified for all the tested specimens.

Numerical simulation: a numerical study was also performed in the framework of the ATTEL RFCS project. A detail description of this study, which is summarised here below can be found in [13]. For this study, LAGAMINE, a nonlinear finite element code developed at Liege University [14], was used to perform the numerical simulations in which geometrical nonlinearities including large deformation and material nonlinearities were taken into account. As the joint is fully symmetric, the computation was carried out on only ¼ of the considered joint as shown in Fig.8. Moreover, the bolts located in the compression zone of the connection are not introduced in the model as they are not activated. The tube, the end-plate, the weld and the bolts are modelled using 8-node brick BLZ3D elements with reduced integration, while the contact surfaces are modelled using CFI3D elements for which the Coulomb law is applied. The detailed properties of these elements can be found in [14]. Considering the meshing, a quite fine mesh with adaptive element sizes is used to suit the geometry shape of the joint. It is assumed that the washer is fully connected to the bolt head as the relative displacement between them is negligible. Moreover, as there is a gap between the bolt's shank and the inner surface of the hole in the end-plates, it is assumed that no contact force is generated between them. As a consequence, only two contact surfaces are modelled: (i) washer-plate interface with friction (coefficient = 0.25) and (ii) plate-rigid foundation interface with no friction (Fig.8). Regarding the bolt modelling, the Agerskov's length [15] is adopted for the effective length of the bolt shank. With respect to the material modelling, the actual σ-ε curves of the materials are implemented in the numerical models.

Yield line analysis: a computer program solving the optimal solution of Eq.(7) was implemented, the strengths of the tested connections are automatic calculated and the so-obtained values are reported in Table 4. In the calculations, both yield and ultimate strengths (i.e. f_y and f_u) are used to compute M_p and M_u respectively.

Experimental and FE analysis comparison: load-displacement curves and the failure modes are compared and reported in Figs. 9 and 10. The connection strengths given by FE analyses are a bit higher than the test ones while the failure mode I is identified for all three specimens in both experimental and FE results. It can be concluded that a good agreement is obtained between the numerical predictions and the experimental results.

Experimental and yield line analysis comparison: plastic and ultimate moments are compared and shown in Figs.11, 12 and 13; it can be observed that a good agreement is obtained. "It is necessary to note that the ultimate moment resistance of the connections can't be reached during the tests because of too large displacement; the maximal moments given by the tests are used to compare with the calculated values."

FE analysis and yield line analysis comparison: the development of the plastic deformations are compared and presented in Fig.14. A rather good agreement is identified in the tension zone while a small difference is observed in the compression zone.

Discussions: the comparisons between the experimental, numerical and analytical results demonstrate that the proposed yield line pattern for the failure mode of the end plate is quite close to the actual one; a good agreement is observed in terms of plastic and ultimate resistances. Accordingly, the proposed analytical model appears to be appropriate.

Remark: the bolt size has influence on the plastic capacity of the end-plate through the yield lines passing the bolt positions. Then, the bolt size effect should be considered in many cases where the effect is significant. For example, with a standard T-stub and the failure mode I is concerned, there are two yield lines (equal to 50% total length of all yield lines) influenced by bolt size leading to a considerable impact. In the present case, the length of yield lines that can be affected by the bolt size is quite small in comparison with the total length of all yield lines (the length of the yield lines 02 and 03 in comparison with the total length of all yield lines in Fig.5). Therefore, the effect of the bolt size in the investigated case may be neglected.

2.4.2. Validation of the approximate solution by comparing to the optimal solution

Considering the optimal solution validated in the previous section as reference results, the results obtained through the simplified approach will be compared to these reference results. The comparison is performed on a series of connections (36 different configurations) for which three parameters are varied (see Fig.15 and Table 5): (1) the ratio between the end-plate width and the tube diameter (b/r = 1.2 to 1.6); (2) the ratio between the height and the width of the end-plate (h/b= 1.0 to 1.6); and (3) the bolt positions(three positions (Fig.15) defined through different values of e_b and e_h (Fig.2b)). The plastic moments ($M_{p,app}$ and $M_{p,opt}$) of the connection given by the approximate and optimal solutions are compared; the obtained results are reported in Table 5. It can be observed from Table 5 that the approximate solution exhibits a rather good agreement with the optimal solution, in particular for configuration with square end-plates; the observed difference increases when the height/width ratio of the rectangular end-plate increases. The mean difference of around 10% demonstrates that the approximate formulas could be proposed for practical applications.

3. Applications

Formulas for the all the mechanisms shown in Fig.3 are now available and may be used to predict the strength of tube-to-tube joints (Fig.1b) and to calculate the force in the bolts in tension of column bases (Fig.1a). The procedure to be followed are given here below.

3.1. For tube-to-tube joints

The results of the proposed model for the joints shown in Fig.3 can be directly applied to determine the plastic strength of the tube-to-tube connections (Fig.1b). As the upper bound approach is adopted, the plastic strength of the joints is the smallest among the values given in Table 6, corresponding to the limit loads of the mechanisms shown in Fig.3. The same formulas may be used to estimate the ultimate strength of the joints if the unit ultimate moment m_u is used instead of m_p, and B_u instead of B_p.

3.2. For column bases

The application of the component method to the column base has been presented in many documents, e.g. [4, 7]. The concrete in compression, the end-plate in bending and the bolts in tension are the three main components of the column bases under bending moment and axial force. How to calculate the concrete in compression component for the column bases with circular tubular column have been presented in many literature, e.g. [9, 16, 17, 18] and they are not reported herein. The tension force in bolts depends on three parameters: (1) the strength of the bolt shanks; (2) the resistance of the end-plate in bending; and (3) the anchorage strength of the bolts in the foundation. It is important to note that the failure in the bolt shanks and in the concrete are not recommended as they lead to a brittle failures. Also, the anchorage failure (bond or cone failure) is not the objective of the present paper, as this master is dealt in the literature, e.g. [19]. The strength of the bolt shanks is known as B_u, and the bending strength of the plate is presented in Section 2. However, many experimental tests demonstrated that the prying forces don't develop in the column bases, due to the important elongation of the anchor bolts (in the case of non-preload bolts). Without the prying forces, the yield lines throughout the bolt positions (Figs.3b and d) cannot develop, and the tension force in bolts can be therefore easily found. In summary, the actual force in bolts located in the tension side of the column bases is the smallest among the value reported in Table 7.

4. Conclusions

A study related to the behaviour of the end plate in bending and bolt in tension components in connections with tubular sections was presented in this paper. A new yield line pattern for the end plate is proposed and developed by using a limit analysis. Analytical formulas for the proposed yield line pattern are proposed and validated through comparisons to experimental and FE results, and that in terms of resistance and failure mode. It was demonstrated that the level of accuracy of the proposed formulas may be sufficient to be proposed for practical situations. The strength of tube-to-tube joints under bending moment can be predicted while the bolt force in the tension zone of a column bases can be determined through the proposed analytical approach.

Acknowledgements

This work was carried out with a financial grant from the Research Fund for Coal and Steel of the European Community, within the ATTEL project: "Performance-Based Approaches for High Strength Steel Tubular Columns and Connections under Earthquake and Fire Loadings", Grant N^0 RFSR-CT-2008-00037.

References

[1] Wardenier J. Kurobane Y., Packer J.A., Dutta D., Yeomans N. Design guide for circular hollow section (CHS) joints under predominantly static loading. CIDECT 2008.

[2] Zhao X.L., Herion S., Packer J.A., Puthli S.R., Sedlacek G., Wardenier J., Weynand K., van Wingerde A.M., Yeomans N.F. Design guide for circular and rectangular hollow section welded joints under fatigue loading. CIDECT 2001.

[3] Eurocode 3: Design of steel structures - Part 1-8: Design of joints. EN 1993-1-8, Brussels, 2003.

[4] Guisse S, Vandegans D, Jaspart JP. Application of the component method to column bases – experimentation and development of a mechanical model for characterization. Research Centre of the Belgian Metalworking Industry, 1996.

[5] Jaspart J.P. Recent advances in the field of steel joints: column bases and future configurations for beam-to-column joints and beam splices. Agregation thesis, University of Liege, 1997.

[6] Wald F., Sokol Z, Jaspart J.P. Base plate in bending and anchor bolts in tension. HERON, Vol. 53 (2008), N^0 2/3.

[7] Wald F., Sokol Z, Steenhuis M., Jaspart J.P. Component method for steel column bases. HERON, Vol. 53 (2008), N^0 2/3.

[8] Wald F., Bouguin V., Sokol Z., Muzeau J.P. Effective length of T-Stub of RHS column base plates. Czech Technical University, 2000.

[9] Horova K., Wald F., Sokol Z. Design of circular hollow section base plates. 6^{th} European Conference on Steel and Composite Structures (EUROSTEEL), Budapest -2011, Vol.A, pp. 249-254.

[10] Wheeler A.T., Clarker M.J., Hancock G.J, Murray T.M. Design Model for Bolted Moment End Plate Connections Joining Rectangular Hollow Sections. Journal of Structural Engineering, Vol. 124, N^0 2, 1998.

[11] Wheeler A.T., Clarker M.J., Hancock G.J. Design Model for Bolted Moment End Plate Connections Joining Rectangular Hollow Sections Using Eight Bolts. Research Report N^0 R827, University of Sydney, 2003.

[12] ATTEL project: "Performance-based approaches for high-strength tubular columns and connections under earthquake and fire loadings", Deliverable Report D.3.1: monotonic and cyclic tests data on base-joint specimens, 2012.

[13] ATTEL project: "Performance-based approaches for high-strength tubular columns and connections under earthquake and fire loadings", Deliverable Report D.5.3: simulation data relevant to the selected typologies of base joints, of HSS-CHS columns and HSS-CFT column and of HSS-concrete composite beam-to-column joints, 2012.

[14] LAGAMINE: User's manual, University of Liege, 2010.

[15] Agreskov H. High strength bolted connections subject to prying. J. Struc Div 1976.

[16] Column base plates. American Institute of Steel Constructions, 2003.

[17] Moore D.B., Wald F (Ed). Design of Structural Connections to Eurocode 3 – Frequently Asked Questions. Czech Technical University, 2003.

[18] Steenhuis M., Wald F., Sokol Z., Stark J. Concrete in compression and base plate in bending. HERON, Vol. 53 (2008), N^0 1/2.

[19] Fastenings to Concrete and Masonry Structures. State of the Art Report, CEB, Thomas Telfort Services Ltd, London 1994, ISBN 0 7277 19378.

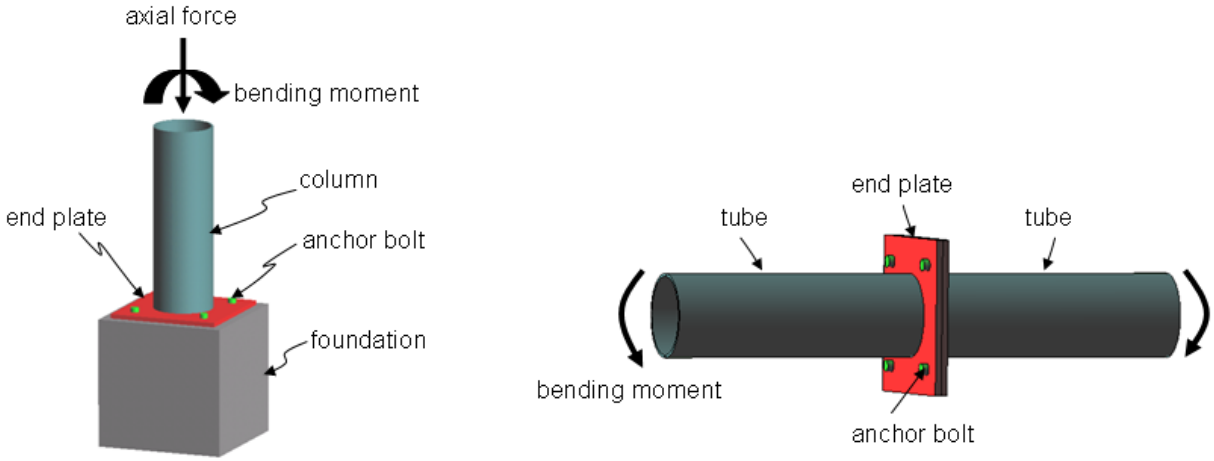

a. Column base b. Tube-to-tube joint

Fig.1. Investigated joints

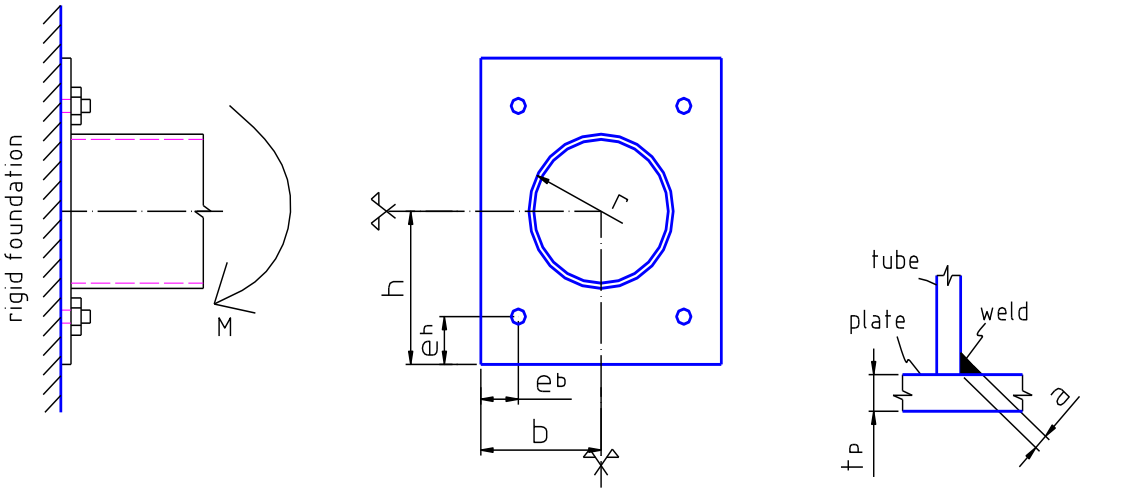

a) limit analysis model b) end-plate geometry c) weld geometry

Fig.2. Geometry and parameters for the limit analysis

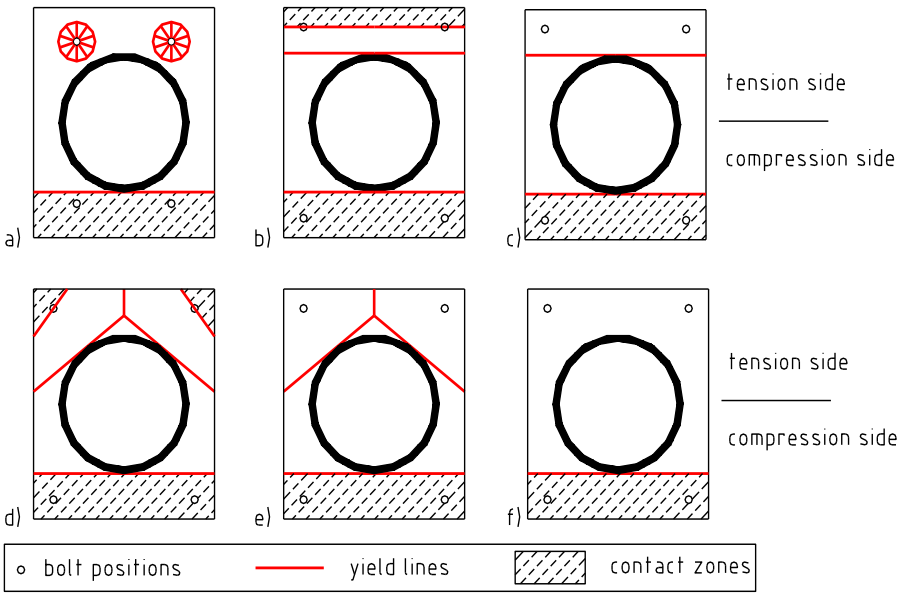

Fig.3. Considered mechanisms

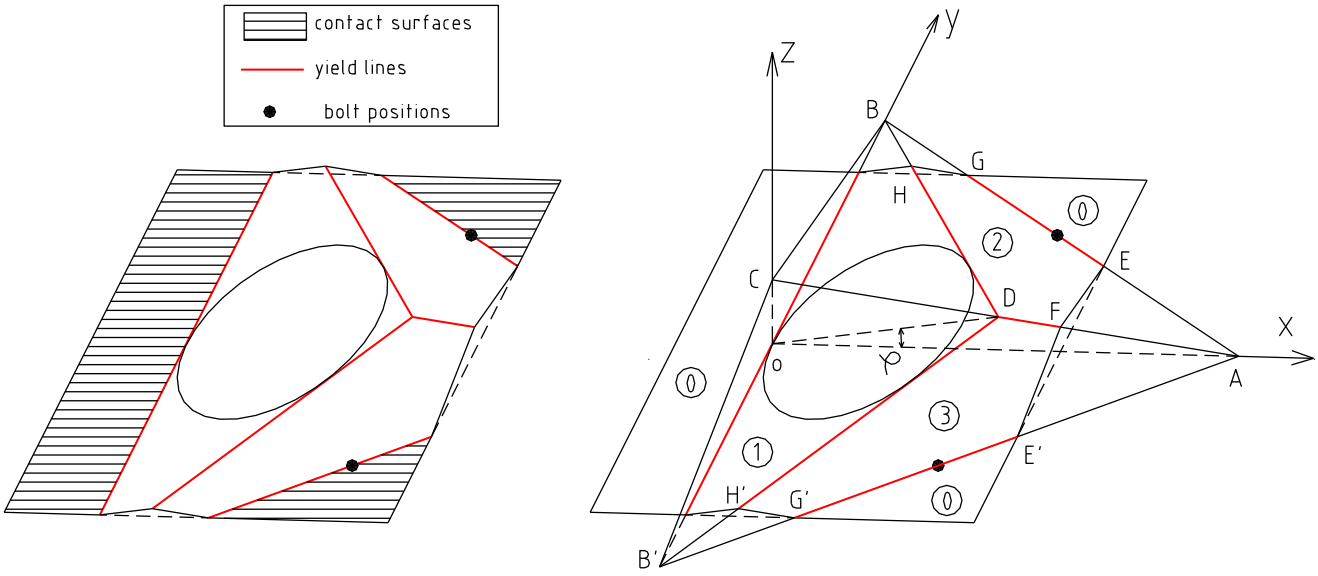

a) plastic mechanism b) detailed geometries

Fig.4. Detailed geometry of yield pattern “d”

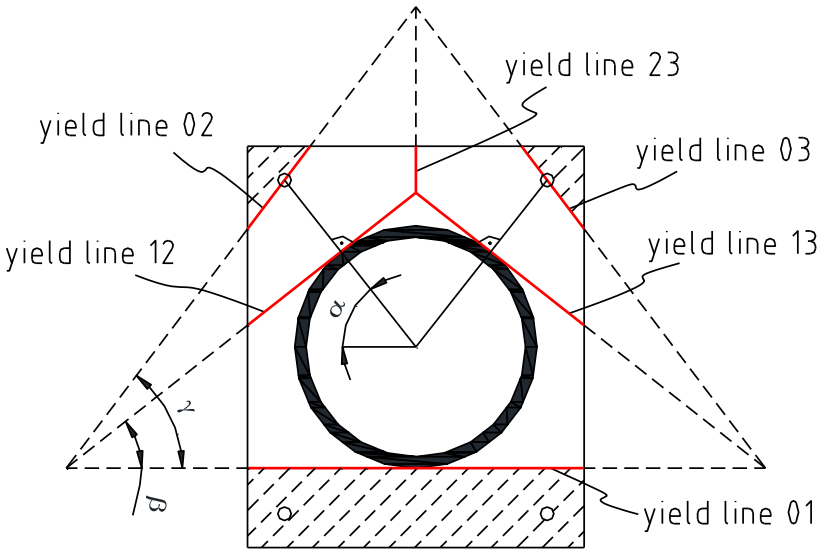

Fig.5. Approximate mechanism of mechanism “d” (Fig.4)

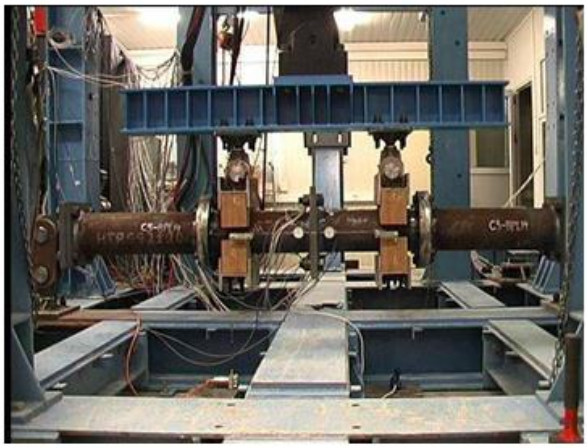

General view

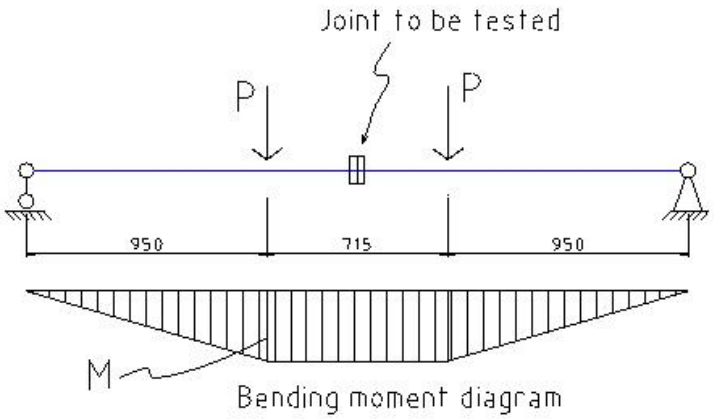

Schema

Fig.6. Test set-up

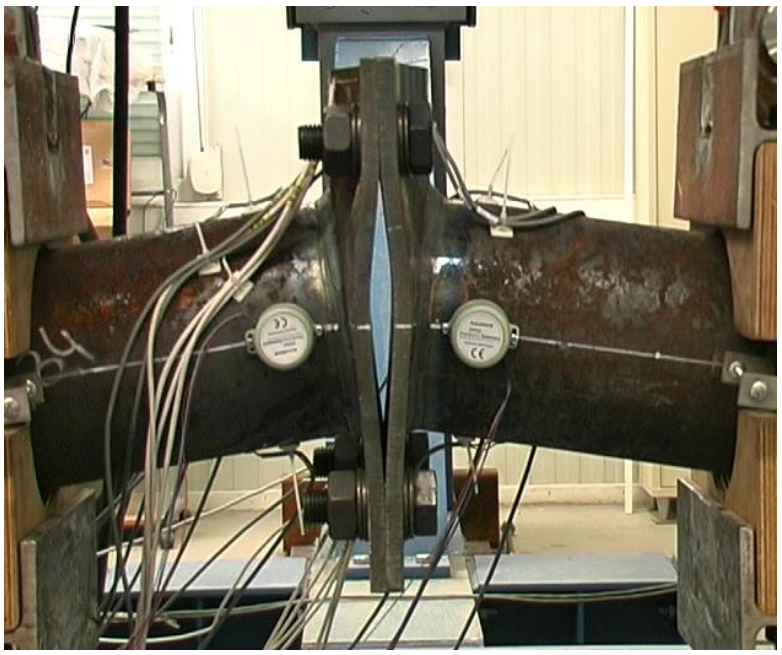

Fig.7. Specimen 1 at the end of the test

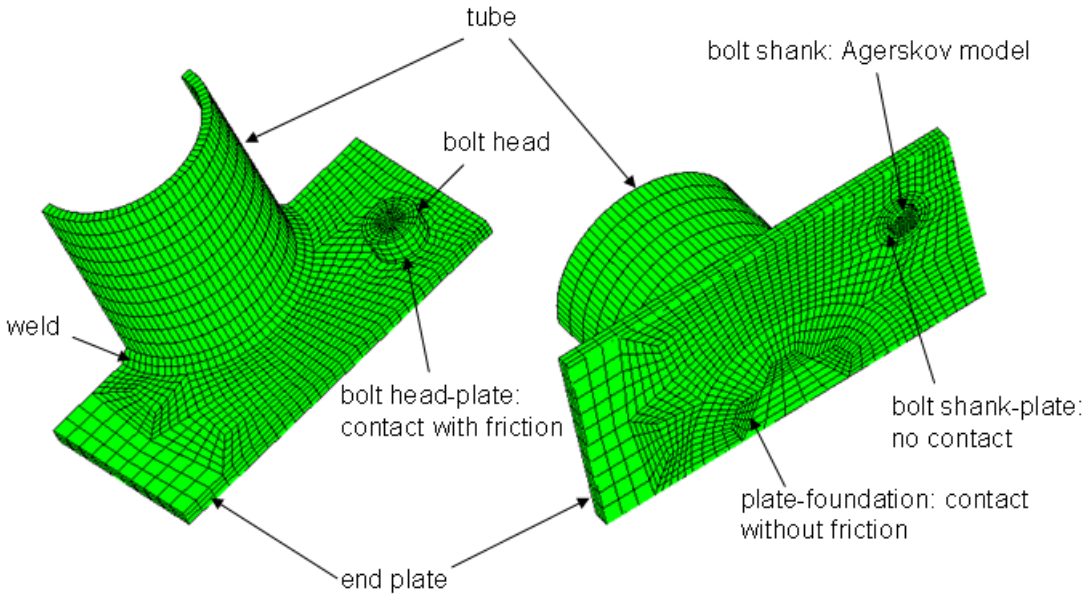

Fig.8. FE modelling of the tested connections (1/4 part)

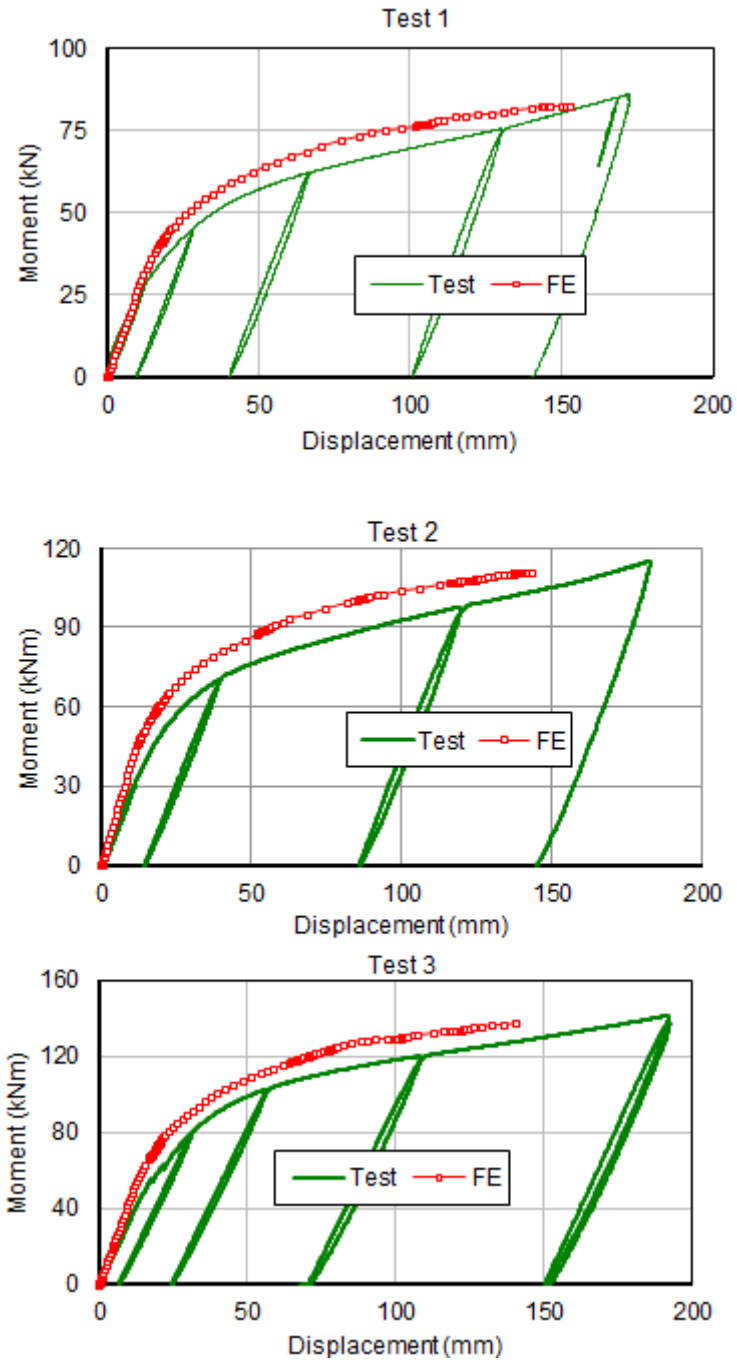

Fig.9. Experimental and FE comparison - load-displacement curves

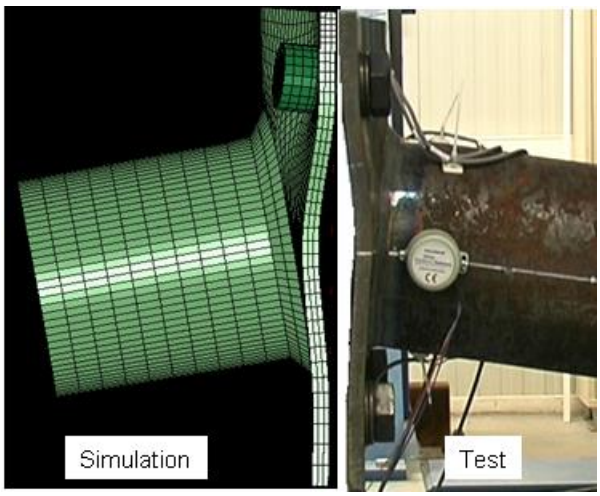

Fig.10. Comparison of the failure mode obtained numerically and experimentally

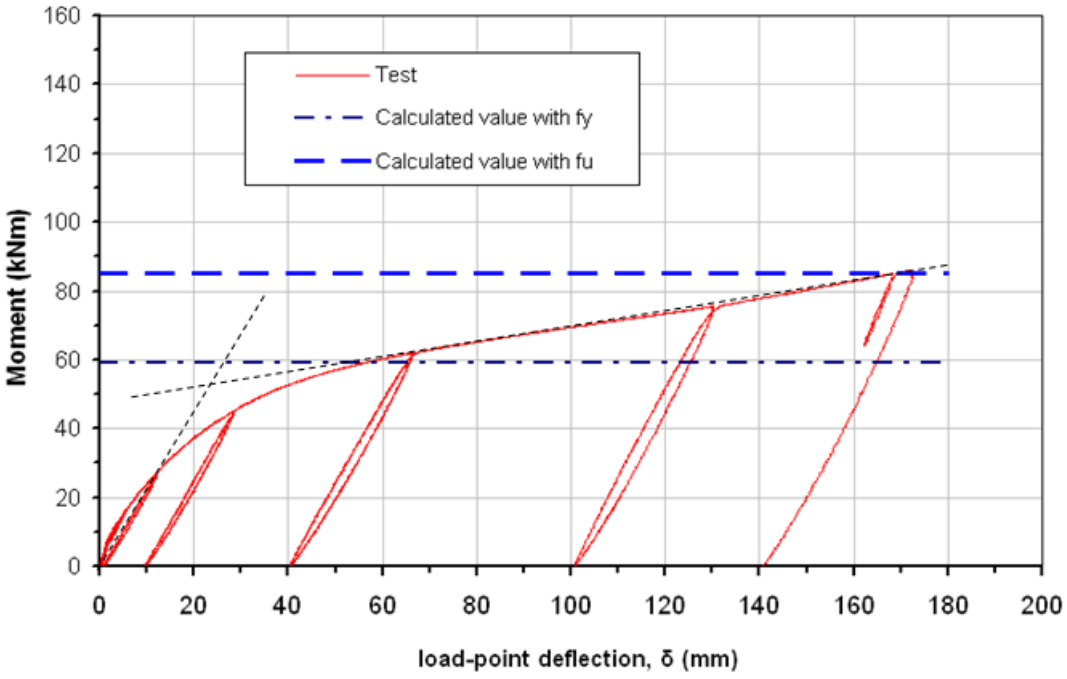

Fig.11. Specimen 1: experimental and analytical comparison

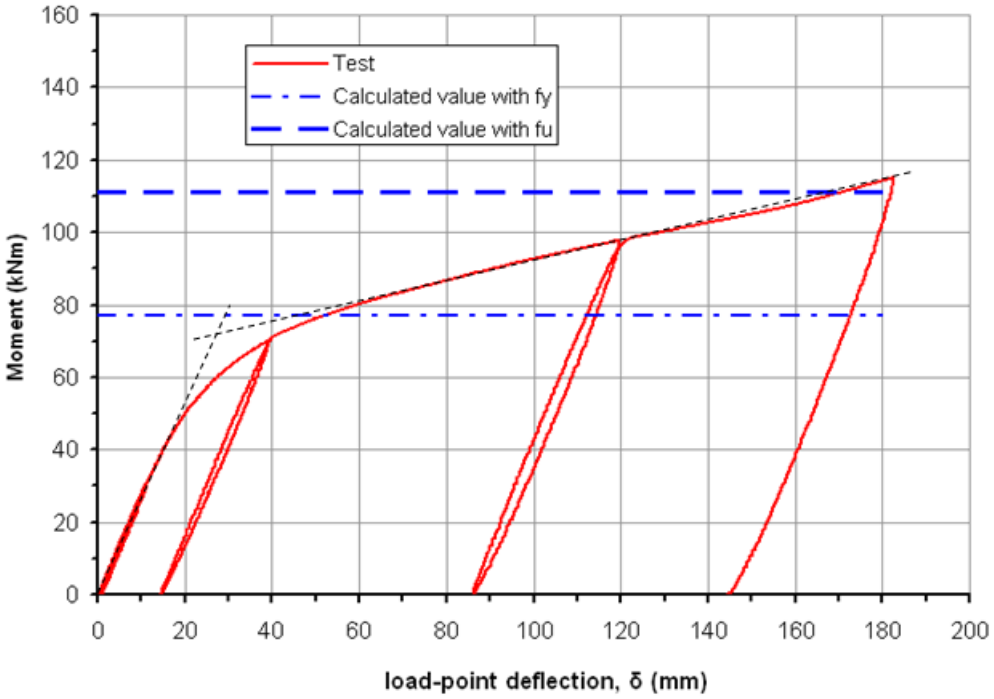

Fig.12. Specimen 2: experimental and analytical comparison

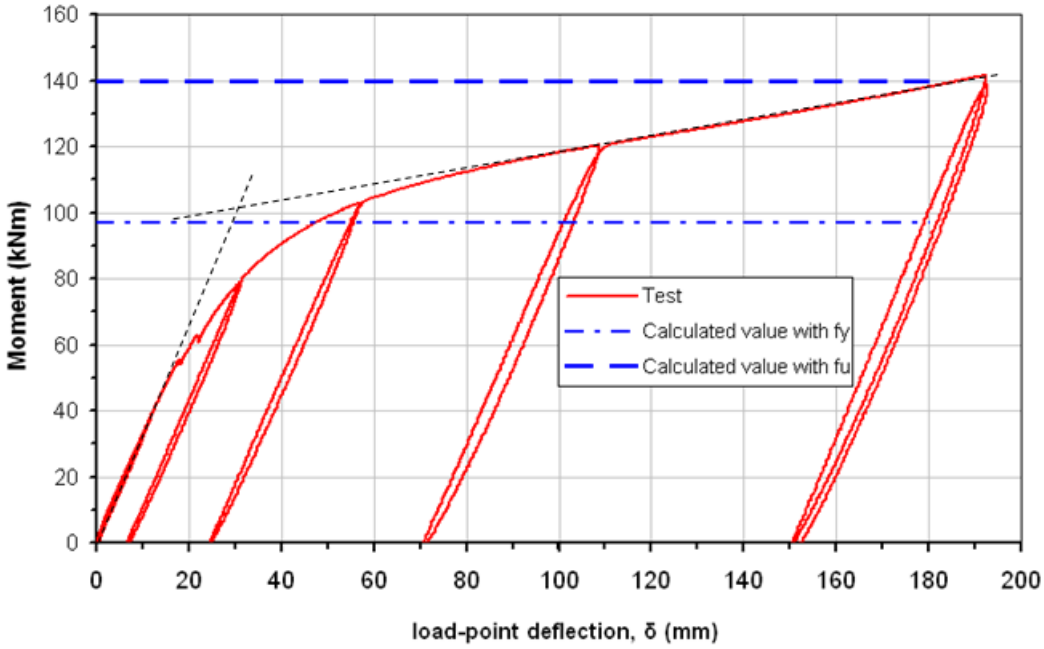

Fig.13. Specimen 3: experimental and analytical comparison

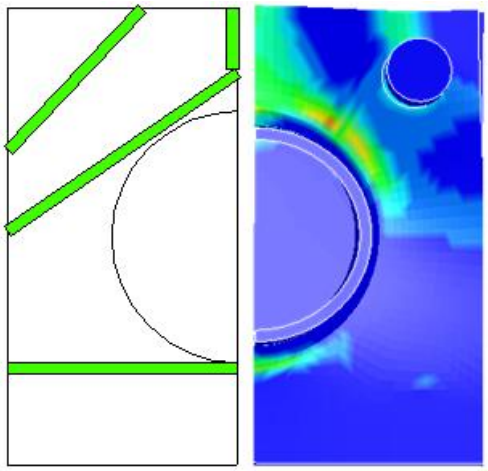

Yield line analysis FE analysis

Fig.14. Analytical and finite element comparison- plastic deformation

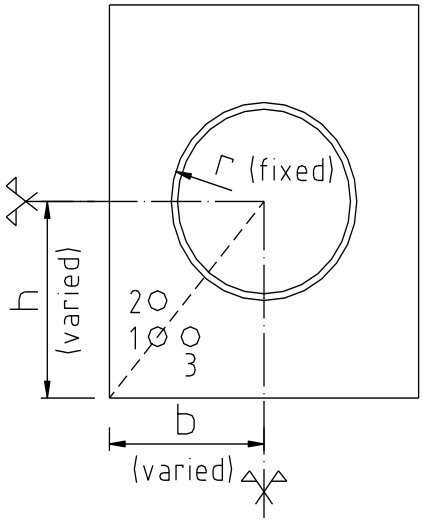

Fig.15. Varied geometrical parameters for the considered connections

Table 1: determination of n_i, n_j, $l_{ij,x}$ and $l_{ij,y}$

plane i – plane j	$\mathbf{n}_i$	$\mathbf{n}_j$	$l_{ij,x}$	$l_{ij,y}$
0-1	$0\mathbf{i}+0\mathbf{j}+1\mathbf{k}$	$-z_D\mathbf{i}+0\mathbf{j}+x_D\mathbf{k}$	0	$y_G - y_{G'}$
0-2	$0\mathbf{i}+0\mathbf{j}+1\mathbf{k}$	$x_A^{-1}\mathbf{i}+y_B^{-1}\mathbf{j}+z_C^{-1}\mathbf{k}$	$x_E - x_G$	$y_G - y_E$
0-3	$0\mathbf{i}+0\mathbf{j}+1\mathbf{k}$	$x_A^{-1}\mathbf{i}+y_{B'}^{-1}\mathbf{j}+z_C^{-1}\mathbf{k}$	$x_{E'} - x_{G'}$	$y_{G'} - y_{E'}$
1-2	$-z_D\mathbf{i}+0\mathbf{j}+x_D\mathbf{k}$	$x_A^{-1}\mathbf{i}+y_B^{-1}\mathbf{j}+z_C^{-1}\mathbf{k}$	$x_D - x_H$	$y_H - y_D$
1-3	$-z_D\mathbf{i}+0\mathbf{j}+x_D\mathbf{k}$	$x_A^{-1}\mathbf{i}+y_{B'}^{-1}\mathbf{j}+z_C^{-1}\mathbf{k}$	$x_D - x_{H'}$	$y_D - y_{H'}$
2-3	$x_A^{-1}\mathbf{i}+y_B^{-1}\mathbf{j}+z_C^{-1}\mathbf{k}$	$x_A^{-1}\mathbf{i}+y_{B'}^{-1}\mathbf{j}+z_C^{-1}\mathbf{k}$	$x_F - x_D$	0

The positions of the points A, B, C, D, E, E', F, G, G', H and H' are shown in Fig.4b.

Table 2: A, C, D, E, E' F, G, G', H and H' coordinates (Fig.4b) as a function of y_B.

Coordinates	**Equations**
x_D	$x_D = r\{1+\cos[2artg(r/y_B)]\}/\cos[2artg(r/y_B)]$
x_A	$x_A = y_B(h-e_h+r)/(y_B-b+e_b)$
z_D	$z_D = \varphi x_D$
$y_{B'}$	$y_{B'} = y_B$
z_C	$z_C = x_A x_D/(x_A - x_D)$
$x_E(=x_{E'})$	$x_E = h+r$
$y_E(=-y_{E'})$	$y_E = y_B(x_A-h-r)/x_A$ (if $x_A < h+r$ then $y_E = 0$)
$x_G(=x_{G'})$	$x_G = x_A(1-b/y_B)$
$y_G(=-y_{G'})$	$y_G = b$
$x_H(=x_{H'})$	$x_H = x_D(y_B-b)/y_B$
$y_H(=-y_{H'})$	$y_H = b$
x_F	$x_F = x_E$

Table 3: geometries and material properties of the tested specimens

Test	Geometries (Fig.2, in mm)						Material (N/mm2)	
	b	h	t_p	r_0	a	e_b=e_h	f_y (yield strength)	f_u (ultimate strength)
1	200	200	14	96.85	16	60	418	602
2	200	200	16	96.85	16	60	418	602
3	200	200	18	96.85	16	60	418	602

Bolts with a diameter of 30mm and a 8.8 grade are used for all specimens.

Table 4: Calculated strength of the tested specimens (using optimal solution)

Test	Plastic moment M_p (kNm)	Ultimate moment M_u (kNm)
1	59	85
2	77	111
3	97	140

Table 5: Validation of the approximate solution

Confi.	Geometries (mm)					Strength (Nmm)		
		b	h	e_b	e_h	$M_{p,\,opt}$	$M_{p,app}$	$M_{p,\,app}/M_{p,\,opt}$
1	300	360	360	73.9	73.9	37721	37608	1.00
2	300	360	360	73.9	88.7	41753	41622	1.00
3	300	360	360	88.7	73.9	42660	42597	1.00
4	300	360	432	84.0	100.8	38133	36519	1.04
5	300	360	432	84.0	120.9	43254	41735	1.04
6	300	360	432	100.8	100.8	41969	40228	1.04
7	300	360	504	92.8	129.9	36478	33988	1.07
8	300	360	504	92.8	155.9	42094	39504	1.07
9	300	360	504	111.4	129.9	39551	36937	1.07
10	300	360	576	100.5	160.8	35192	32147	1.09
11	300	360	576	100.5	193.0	41199	36847	1.12
12	300	360	576	120.6	160.8	37740	33455	1.13
13	300	420	420	103.9	103.9	39965	38018	1.05
14	300	420	420	103.9	124.7	43919	42435	1.03
15	300	420	420	124.7	103.9	44625	42528	1.05
16	300	420	504	114.0	136.8	38341	35520	1.08
17	300	420	504	114.0	164.1	43322	40423	1.07
18	300	420	504	136.8	136.8	41899	39003	1.07
19	300	420	588	122.8	171.9	36965	33624	1.10
20	300	420	588	122.8	206.3	42430	38876	1.09
21	300	420	588	147.4	171.9	39828	36449	1.09
22	300	420	672	130.5	208.8	35868	31057	1.15
23	300	420	672	130.5	250.6	41719	35117	1.19
24	300	420	672	156.6	208.8	38240	31960	1.20
25	300	480	480	133.9	133.9	41045	37429	1.10
26	300	480	480	133.9	160.7	45496	41673	1.09
27	300	480	480	160.7	133.9	45224	41708	1.08
28	300	480	576	144.0	172.8	39340	35459	1.11
29	300	480	576	144.0	207.3	44322	40190	1.10
30	300	480	576	172.8	172.8	42638	38805	1.10
31	300	480	672	152.8	213.9	38036	33897	1.12
32	300	480	672	152.8	256.7	43470	38480	1.13

33	300	480	672	183.4	213.9	40688	35548	1.14
34	300	480	768	160.5	256.8	36999	30680	1.21
35	300	480	768	160.5	308.2	42802	34489	1.24
36	300	480	768	192.6	256.8	39185	31470	1.25
						The mean difference:		10%

Table 6: plastic resistance for the tube-to-tube joints

Yield pattern	Failure mode	Plastic strength (M_{pi})
Fig.3a	Mode 1– thin plate	$M_{p1} = [8\pi(h + r - e_h) + 2b]m_p$
Fig.3b	Mode 1– thin plate	$M_{p2} = 4(\frac{2r}{h - r - e_h} + 1)bm_p$ (*)
Fig.3c	Mode 2 – intermediate plate	$M_{p3} = 4\left(1 + \frac{r}{h - r}\right)bm_p + 4\frac{re_h}{h - r}B_p$
Fig.3d	Mode 1- thin plate	$M_{p4} = M_p^I$ (Eq.(8))
Fig.3e	Mode 2 – intermediate plate	$M_{p5} = M_p^{II}$ (Eq.(9))
Fig.3f	Mode 3 – thick plate	$M_{p6} = M_p^{III}$ (Eq.(10))

Remark: (*) only applied for the cases where $h - r - e_h > 0$.

Table 7: determination of the tension in the bolt, F_b (for one bolt)

Yield pattern in tension zone	Failure mode	Bolt force F_b (one bolt)
Circular (Fig.3a)	Mode I- thin plate	$F_{b1} = 4\pi m_p$
Perpendicular (Fig.3c)	Mode I – thin plate	$F_{b2} = \frac{b}{h - r - e_h}m_p$
Incline (Fig.3e)	Mode I- thin plate	$F_{b3} = \frac{(\theta_{12}l_{12} + 0.5\theta_{23}l_{23})m_p}{h + r - e_h}$ (*)
-	Mode III– thick plate	$F_{b4} = B_p$

Remarks: (*) θ_{12}, θ_{23}, l_{12}, l_{23} are determined through Eqs. (12), (14), (16) and (18) respectively.